

Accessing the pion 3D structure at US and China Electron-Ion Colliders

José Manuel Morgado Chávez,^{1,*} Valerio Bertone,^{2,†} Feliciano De Soto Borrero,^{3,‡} Maxime Defurne,^{2,§}
Cédric Mezrag,^{2,¶} Hervé Moutarde,^{2,**} José Rodríguez-Quintero,^{1,††} and Jorge Segovia^{3,‡‡}

¹*Department of Integrated Sciences and Center for Advanced Studies in Physics,
Mathematics and Computation, University of Huelva, E-21071 Huelva, Spain*

²*Irfu, CEA, Université Paris-Saclay, 91191, Gif-sur-Yvette, France*

³*Dpto. Sistemas Físicos, Químicos y Naturales,
Universidad Pablo de Olavide, E-41013 Sevilla, Spain*

(Dated: January 3, 2022)

We present in this letter the first systematic feasibility study of accessing generalised parton distributions of the pion at an electron-ion collider through deeply virtual Compton scattering at next-to-leading order. It relies on a state-of-the-art model, able to fulfil by construction all the theoretical constraints imposed on generalised parton distributions. Strikingly, our analysis shows that quarks and gluons interfere destructively and that gluon dominance could be spotted by a sign change of the DVCS beam spin asymmetry.

INTRODUCTION

Due to its double role of being both a Goldstone boson of the chiral symmetry breaking and a QCD bound state, the pion has been widely investigated since its discovery in 1947. In the 1980s and after, many efforts have been done to extract experimental information about its internal structure, from its electromagnetic form factor (EFF) through pion-electron scattering [1] to its parton distribution functions (PDFs) through the Drell-Yan process [2–4]. The latter has in fact triggered a controversy on the PDF large- x behaviour which remains not completely solved today, despite modern phenomenological and theoretical progresses [5–8]. However, using the available pion sources, EFF measurements are limited to low momentum transfer, precluding the possibility to test perturbative-QCD (pQCD) predictions [9, 10]. Exploiting the ideas of Sullivan [11], consisting of interacting with the meson cloud of the proton, EFF data at significantly larger values of the momentum transfer between the virtual and real pion have been obtained [12]. This same principle is being seriously considered both for improving the knowledge on the pion EFF and to extract the PDFs of the pion in the context of the forthcoming US and Chinese Electron Ion Collider (EIC and EicC) [13–15]. The question has raised sufficient interest so that the EIC Yellow Report [16] mentions the study of the 3D structure of the pion through the Sullivan process. The present paper is a quantitative assessment of the latter.

The 3D structure [17] of the pion can be gained through Generalised Parton Distributions (GPDs) [18–22]. Throughout the years, many models for pion’s GPDs have been developed [23–35], including in the crossed channel [36]. They rely on various physics assumptions and if feasible, Deep Virtual Compton Scattering (DVCS) [19] off the pion would provide key constraints on these models [37–39].

In this paper, relying on the implementation of the

state-of-the-art model for pion’s GPD presented in section 2, we compute in section 3 the Sullivan amplitude at Next-to-Leading Order (NLO), the minimal order required to treat the EIC kinematical region. In section 4, we evaluate the associated counting rate and assess the asymmetries, concluding that, providing that the one-pion exchange is the dominant process, DVCS off a virtual pion will be measurable and will provide a clear signal for a glue-dominated regime ideal to “understand the glue that binds us all”.

MODELLING GPDS

Among all available pion’s GPD models, we chose the one presented in Ref. [39], a kinematical completion of that featured in [35] owing to a long effort developed over the last decade [24–27, 30, 31]. In a nutshell, this model is built on the state-of-the-art Continuum Schwinger Methods (CSM) investigations [40–46] which have already provided the community with Parton Distributions Functions (PDFs) in agreement with the large- x behaviour extracted from experimental data including soft-gluon (threshold) resummation [7, 8]; and are confirmed both in the quark and gluon sectors [47, 48] by lattice QCD computations.

The leap from quark PDFs q_π to quark GPDs H_π^q is however made difficult because their dependences on x , the average momentum fraction of the active parton in the pion, ξ , half of the exchanged longitudinal momentum fraction, and t_π the square of the total momentum transfer are constrained by a set of properties [49, 50]. To ensure that all properties are satisfied by construction, we turn to the lightfront wave function formalism [51] (see also [52–56] for details of the connection between CSM and lightfront physics) supplemented by the so-called GPD covariant extension [30, 31]. Our quark

GPD in the DGLAP ($|x| \geq |\xi|$) region reads [39]:

$$H_\pi^q(x, \xi, t_\pi)|_{x \geq |\xi|} = \sqrt{q_\pi(x_{in}) q_\pi(x_{out})} \Phi_\pi^q(x, \xi, t_\pi) \quad (1)$$

with

$$q_\pi(x) = \mathcal{N}_q x^2 (1-x)^2 \left[1 + \gamma x (1-x) + \rho \sqrt{x(1-x)} \right], \quad (2)$$

$$\Phi_\pi^q(x, \xi, t_\pi) = \frac{1}{4} \frac{1}{1+\zeta^2} \left(3 + \frac{1-2\zeta}{1+\zeta} \frac{\operatorname{arctanh}\left(\sqrt{\frac{\zeta}{1+\zeta}}\right)}{\sqrt{\frac{\zeta}{1+\zeta}}} \right), \quad (3)$$

$$\zeta = -\frac{t_\pi}{4M^2} \frac{(1-x)^2}{1-\xi^2}, \quad x_{in} = \frac{x+\xi}{1+\xi}, \quad x_{out} = \frac{x-\xi}{1-\xi}; \quad (4)$$

modeled at a low reference scale $\mu_{\text{Ref}} = 331 \text{ MeV}$, defined as discussed in [45, 46]. The PDFs parameters obtained in [43] are $\mathcal{N}_q = 213$, $\gamma = 2.29$ and $\rho = -2.93$. The covariant extension provides us with the corresponding ERBL ($|x| \leq |\xi|$) region. Evolution equations from μ_{Ref} up to experimental scales are applied in the scheme introduced in [35, 43, 45], generating accordingly the gluon GPDs, which are crucial ingredients in any EIC-related study. The latter yields in the forward limit a gluon PDF in excellent agreement with the one computed on the lattice [47, 48]. This theoretical framework is reinforced by information coming from experimental extractions of EFF [12], fixing $M = 318 \text{ MeV}$.

In the case of the Sullivan process, one should consider a *transition* GPD between a virtual and a real pion. However, for low enough virtuality, it has been shown [57, 58] that extrapolations from the standard GPD are possible. Therefore, virtuality effects are neglected in the chosen GPD model. This relies on a previous work on the pion EFF [57], indicating that neglecting virtualities tends to yield a smaller signal at non-vanishing momentum transfer, thus not undermining our conclusion on the feasibility of the measurement.

DVCS THROUGH THE SULLIVAN PROCESS

The DVCS amplitude is parametrised by a Compton Form Factor (CFF), a convolution of the pion GPD and a hard kernel computable within pQCD. At leading order (LO), the latter selects only quark GPDs, while at NLO, an exchange of a gluon pair in t -channel is allowed [59–62]. Another competing process, called Bethe-Heitler (BH), leads to the same final state as DVCS except that the real photon is emitted by either the incoming or outgoing lepton. As a consequence the cross section for photon electroproduction off a pion

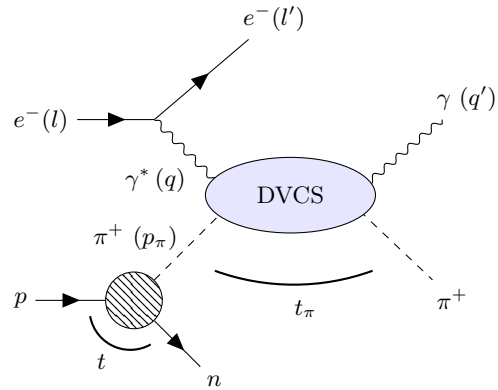


FIG. 1. DVCS off a virtual pion through the Sullivan process: The virtual pion from the proton absorbs the virtual photon γ^* and subsequently emits a real photon γ while turning itself real. The kinematical variables are defined as follows: $Q^2 = -q^2$, $y = \frac{p \cdot q}{p \cdot l}$, $y_\pi = \frac{p_\pi \cdot q}{p_\pi \cdot l}$ and $x_B^\pi = \frac{Q^2}{2p_\pi \cdot q}$.

$e\pi \rightarrow e\pi\gamma$ is the coherent sum of both processes amplitudes:

$$\frac{d^5\sigma^{e\pi \rightarrow e\gamma\pi}(\lambda, \pm e)}{dy_\pi dx_B^\pi dt_\pi d\phi d\phi_e} = \frac{d^2\sigma_0}{dQ^2 dx_B^\pi} \frac{1}{\epsilon^6} \times \left[|\mathcal{T}^{BH}|^2 + |\mathcal{T}^{DVCS}|^2 \mp \mathcal{I}(\lambda) \right], \quad (5)$$

$$\frac{d^2\sigma_0}{dQ^2 dx_B^\pi} = \frac{\alpha_{QED}^3 x_B^\pi y_\pi}{16\pi^2 Q^2 \sqrt{1+\epsilon^2}}, \quad (6)$$

$$\epsilon^2 = 4m_\pi^2 (x_B^\pi)^2 / Q^2, \quad (7)$$

$$\mathcal{I}(\lambda) = \mathcal{I}_{\text{unp}} + \lambda \mathcal{I}_{\text{pol}}; \quad (8)$$

where \mathcal{T}^{BH} stands for the BH amplitude, \mathcal{T}^{DVCS} for the DVCS amplitude and $\mathcal{I}_{\text{unp/pol}}$ for the un-/polarized interference terms. λ is the electron helicity, $-e$ its charge, α_{QED} the electromagnetic coupling, ϕ_e the azimuthal angle of the scattered lepton, m_π the mass of the pion and ϕ the angle between the leptonic plane and the hadronic plane, defined according to the Trento convention [63]. While the squared DVCS amplitude gives access to the modulus of the CFF, its real and imaginary parts are independently accessible thanks to the interference term. In order to compute CFFs from the GPD model introduced above, we took advantage of PARTONS [64] where the formulae of Refs. [61, 62] are implemented, together with Apfel++ [65–67] providing us with a LO evolution routine for GPDs.

Two additional variables are required to characterise the virtual pion in the initial state: $x_\pi = \frac{p_\pi \cdot l}{p \cdot l}$ being the fraction of the proton energy carried by the virtual pion in the ep center-of-mass frame and $t = p_\pi^2$. Following the formulae in Ref. [68], the cross section of the Sullivan

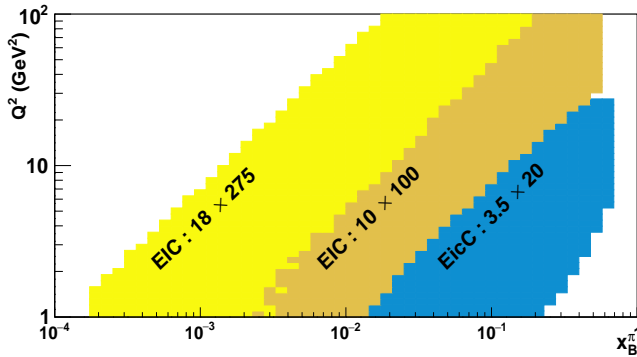


FIG. 2. Phase space in x_B^π and Q^2 considered in the present study: Facilities and configurations (electrons \times protons beams energies in GeV) contributing the most to the statistics in the colored areas are specified.

process (see Fig. 1) then reads:

$$\frac{d^8 \sigma^{\text{Sul}}(\lambda, \pm e)}{dy dQ^2 dt_\pi d\phi d\phi_e dt dx_\pi d\phi_n} = x_\pi \frac{g_{\pi NN}^2}{16\pi^3} F(t)^2 \frac{-t}{(m_\pi^2 - t)^2} |J_{x_B^\pi}^{Q^2}| \frac{d^5 \sigma^{e\pi \rightarrow e\gamma\pi}(\lambda, \pm e)}{dy_\pi dx_B^\pi dt_\pi d\phi d\phi_e} \quad (9)$$

with $J_{x_B^\pi}^{Q^2}$ the Jacobian between Q^2 and x_B^π , ϕ_n the azimuthal angle of the spectator neutron and $g_{\pi NN} = 13.05$ being the pion-nucleon coupling constant. Amrath *et al.* introduced a phenomenological factor $F(t)$ in Ref. [68] to reduce the pion-nucleon vertex as $|t|$ increases. The latter takes the form:

$$F(t) = \frac{\Lambda^2 - m_\pi^2}{\Lambda^2 - t}, \quad (10)$$

with $\Lambda = 800$ MeV. Finally, we stick to a chiral limit description of the pion, neglecting its mass in Eq. (5) and associated equations from Ref. [69].

In order to ensure a proper interpretation of the event as a Sullivan DVCS process, the pion virtuality $|t|$ must be small enough and will be taken such that $|t| \leq |t|_{\text{max}} = 0.6 \text{ GeV}^2$ as well as $s_\pi = (p_\pi + q)^2 > s_\pi^{\text{min}} = 4 \text{ GeV}^2$ [68]. In addition, to reduce the contribution from nucleon resonances N^* through the process $ep \rightarrow eN\gamma \rightarrow en\pi\gamma$, the invariant mass of the $n\pi$ -system is required to be larger than 2 GeV. For the sake of completeness, let us mention that there also are contributions which cannot be easily restricted by cutting on kinematical variables. For instance, virtual ρ 's may contribute as well through $\gamma^*\rho \rightarrow \gamma\pi$ and can only be assessed with a model of transition form factors and GPDs. We neglect them in the present study.

EVALUATION OF OBSERVABLES

Both EIC and EicC facilities will deliver highly polarised lepton and hadron beams. Their characteristics

	EIC	EicC
Lepton beam energy (GeV)	5/10/18	3.5
Hadron beam energy (GeV)	41/100/275	20
Lepton polarization	70%	80%
Hadron polarization	70%	70%
Integrated luminosity ($\text{fb}^{-1}/\text{year}$)	10	50

TABLE I. Main characteristics of both electron-ion colliders obtained from Ref. [16] (EIC) and Ref. [15] (EicC).

are summarised in Table I and the coverage they offer is illustrated on Fig. 2.

Regarding the EIC's design [16], a central barrel detector, with two end-caps sitting in a 3T solenoidal magnetic field, will be in charge of spotting the scattered lepton, the photon and the recoil pion with pseudo-rapidity between -4 to 4 . For the purpose of this study, it is worth mentioning that a far-forward spectrometer will detect the recoil pion with polar angle between 6 and 20 mrad. A Zero-Degree calorimeter will detect the neutron with polar angles from 0 to 5.5 mrad.

Equivalently, the design of the EicC [15] is composed of a central and far-forward detector package. However, as the EicC is still at a conceptual stage, key parameters for our study are not provided such as the acceptance for the neutron. Hence, we will assume an ideal geometry for the EicC spectator neutron tagger.

To guarantee the exclusivity, a reliable detection/identification of the electron, the photon and the neutron is assumed. Momentum conservation will be required and therefore pion identification is not considered as mandatory.

The number of events is then estimated by Monte-Carlo simulation. As seen in Eq. (9), five kinematical variables and three angles are necessary to fully determine the final state. They are all uniformly generated in a range whose boundaries are controlled by previously generated variables, together with cuts guaranteeing the validity of the Sullivan process following Ref. [68]. For each event, the generation starts with x_π and t to determine the virtual pion. Lower and upper bounds for x_π are defined as follows:

$$x_\pi^{\text{min}} = \frac{1}{y_{\text{max}}} \frac{s_\pi^{\text{min}} + Q_{\text{min}}^2}{s}, \quad (11)$$

$$x_\pi^{\text{max}} = \frac{1}{2} \left[\sqrt{\tau^2 + 4\tau} - \tau \right], \quad (12)$$

with $\tau = |t|_{\text{max}}/M_N^2$. Then t is generated between $-|t|_{\text{max}}$ and $-|t|_{\text{min}} = \frac{x_\pi^2 M_N^2}{1-x_\pi}$, with M_N being the nucleon mass. To complete the determination of the virtual pion and neutron spectator, a rotation of an angle $\phi_N \in [0; 2\pi]$ around the incoming proton is performed. Then, the values of Q^2 and y are generated, providing us with the virtual photon. Considering that cross sections are too low above $Q^2 = 100 \text{ GeV}^2$, Q_{max}^2 is given

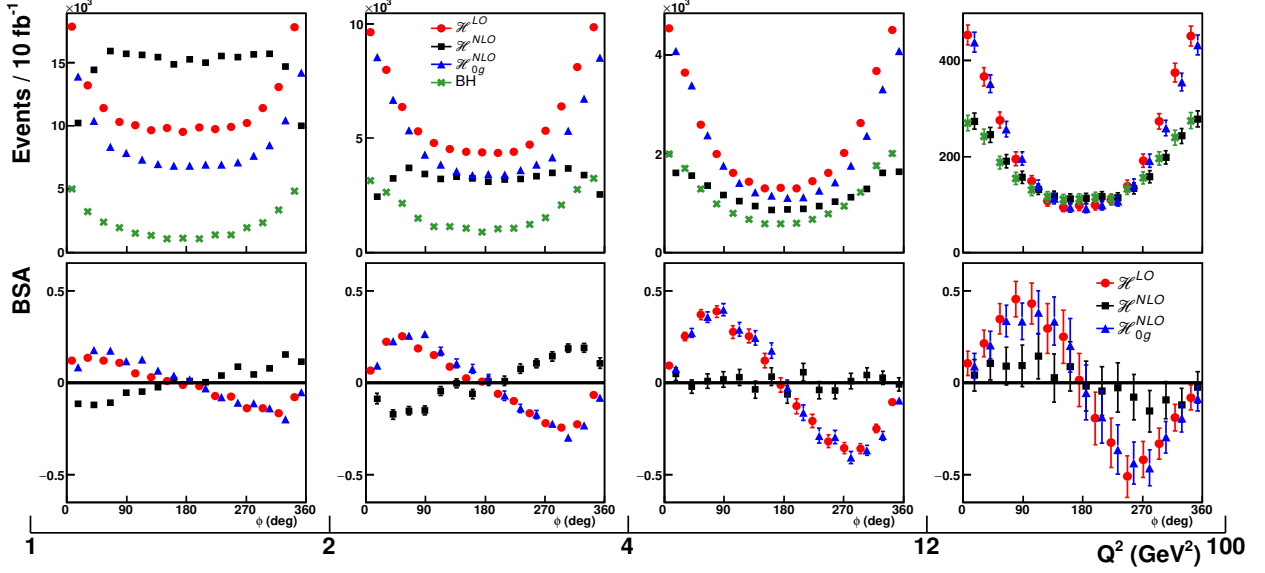


FIG. 3. Number of DVCS events (upper charts) and expected beam-spin asymmetries (lower chart) as a function of Q^2 for $x_B^\pi \in [10^{-3}; 10^{-2}]$. Red circles: LO evaluation of the CFF; blue triangles: NLO evaluation but without taking gluon GPDs into account; black circles: full NLO results. The BH event rates is as well displayed by the green crosses.

by:

$$Q_{max}^2 = \min(s x_\pi^{max} y_{max} - s_\pi^{min}, 100), \quad (13)$$

with $s = (p + l)^2$. The upper bound for the inelasticity y is set to 0.85 [68], while the lower bound is given by:

$$y_{min} = \frac{1}{x_\pi} \frac{s_\pi^{min} + Q_{min}^2}{s}. \quad (14)$$

Then the virtual photon and the scattered lepton are rotated around the incoming lepton by the angle $\phi_e \in [0; 2\pi]$.

Finally, the variable t_π lies within the range $t_\pi^{max} = -0.6 \text{ GeV}^2$ and t_π^{min} computed exactly, *i.e.* taking into account the virtuality of the initial state pion. A last rotation around the virtual photon axis in the $\gamma^* \pi$ -system is performed for ϕ . In order to correct for the non-uniformity of the event generation across the entire phase space, each event i must be weighted by a phase space factor $d\Psi^i$ defined as:

$$d\Psi^i = \frac{1}{N_{gen}} \prod_{k \in \mathcal{K}} k_{max}^i - k_{min}^i, \quad (15)$$

with $\mathcal{K} = \{Q^2, y, t, x_\pi, t_\pi, \phi_e, \phi_N, \phi\}$ and N_{gen} the number of generated events. The number of expected events \mathcal{N} is then obtained by:

$$\mathcal{N} = \mathcal{L} \sum_{i \in \Phi} \frac{d^8 \sigma^i(\lambda, \pm e)}{dy dQ^2 dt_\pi d\phi d\phi_e dt dx_\pi d\phi_n} \times d\Psi^i, \quad (16)$$

where Φ is the phase space of events passing kinematical cuts with all final state particles detected, and \mathcal{L} the integrated luminosity over a year (see Tab. I).

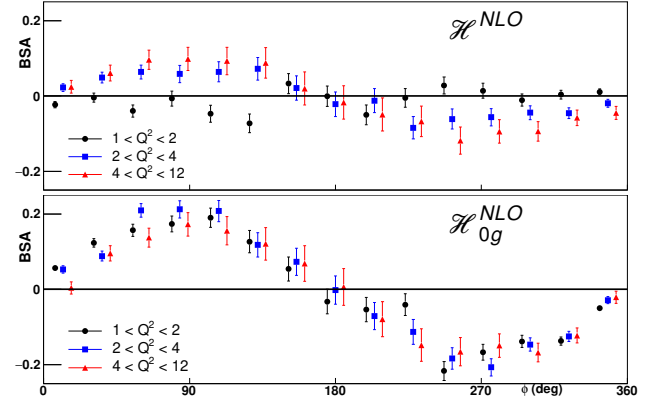


FIG. 4. Expected beam-spin asymmetries as function of ϕ with \mathcal{H}^{NLO} (top) and \mathcal{H}_{0g}^{NLO} (bottom) from EicC for $x_B^\pi \in [0.1; 0.5]$ and three different Q^2 -bins: black circles for Q^2 between 1 and 2 GeV^2 , blue squares between 2 and 4 GeV^2 , and red triangles between 4 and 12 GeV^2 .

Three scenarii are compared with CFF- \mathcal{H} computed at LO (\mathcal{H}^{LO}), at NLO with (\mathcal{H}^{NLO}) and without (\mathcal{H}_{0g}^{NLO}) the contribution of the gluon GPD. From Fig. 3 presenting expected count rates and Beam Spin Asymmetries (BSA) for $x_B^\pi \in [10^{-3}; 10^{-2}]$ and 4 different Q^2 -bins, several conclusions can be drawn. First, we obtain event-rates clearly not compatible with the sole BH contribution, highlighting the possibility of accessing DVCS on a pion target at future electro-ion colliders. Second, \mathcal{H}^{LO} and \mathcal{H}_{0g}^{NLO} -predictions are similar, therefore the NLO corrections to the quark amplitude are small. On the contrary, the \mathcal{H}^{NLO} -CFF which in-

cludes gluons offers substantially different predictions compared to \mathcal{H}_{0g}^{NLO} -CFF for both event rates and beam spin asymmetries. The gluon contribution to the CFF has an opposite sign to the quark one, resulting in a destructive interference. This destructive interference is clearly visible for Q^2 above 12 GeV², with the expected statistics dropping to the BH-only signal and the BSA being reduced by more than a factor 2. As Q^2 decreases, the gluonic contribution dramatically increases: the BSA changes sign and the expected statistics with gluons gets even much higher than the quark-only signal for $Q^2 < 2$ GeV² despite the interference. Our model predicts that the BSA sign change will be clearly visible at the EIC, being a smoking gun for pinning down the transition between quark and gluon dominance in the DVCS description.

Remarkably, the gluon contribution remains sizeable in the valence region accessible through EicC (see Fig. 2) with high statistical accuracy as shown in Fig. 4. At NLO and without the gluon contribution in the valence region, the BSA amplitude does not change much as a function of Q^2 and reaches about 0.2. Contrarily, when the gluon GPD is considered, it almost vanishes at low Q^2 and rapidly increases with Q^2 but remains smaller by a factor 2 compared to the gluonless case.

CONCLUSION

In this paper, we have studied the possibility to probe experimentally the pion 3D structure through the Sullivan process. Using a state-of-the-art model based on Continuum Schwinger Methods, we obtained for one year of integrated luminosity at EIC and EicC a significant number of events. It shows that DVCS off a virtual pion will be measurable, providing that the one-pion exchange is the dominant process. Although focusing in this article on Q^2/x_B^{π} -dependence, the statistics should be high enough to study the t -dependence as well. We also highlighted a smoking gun for gluon dominance of the DVCS cross section; namely that the beam spin asymmetry changes sign because of destructive interferences between quarks and gluons. The wide kinematical coverage coupled with the high luminosity of EIC and EicC should allow us to see this effect. Since the role of the two gluons exchange in the t -channel becomes dominant, next-to-next-to-leading order corrections to the DVCS kernel [70] are certainly desirable, and may confirm the behaviour highlighted here at NLO.

We would like to thank P. Barry, H. Dutrieux, T. Meisgny, B. Pire, K. Raya, C.D. Roberts, Q.-T. Song, P. Sznajder and J. Wagner for interesting discussions and stimulating comments. This work is supported by University of Huelva under grant EPIT-2019 (J.M.M.C). F.S., J.R.Q. and J.S. acknowledge support from Ministerio de Ciencia e Innovación (Spain) under grant PID2019-107844GB-C22; Junta de Andalucía, under

contract No. operativo FEDER Andalucía 2014-2020 UHU-1264517 and P18-FR-5057 and PAIDI FQM-370. This project was supported by the European Union's Horizon 2020 research and innovation programme under grant agreement No 824093. This work is supported in part in the framework of the GLUODYNAMICS project funded by the "P2IO LabEx (ANR-10-LABX-0038)" in the framework "Investissements d'Avenir" (ANR-11-IDEX-0003-01) managed by the Agence Nationale de la Recherche (ANR), France.

* josemanuel.morgado@dcu.uhu.es

† valerio.bertone@cea.fr

‡ fcsotbor@upo.es

§ maxime.defurne@cea.fr

¶ cedric.mezrag@cea.fr

** herve.moutarde@cea.fr

†† jose.rodriguez@dfeie.uhu.es

‡‡ jsegovia@upo.es

- [1] S.R. Amendolia et al. A Measurement of the Space - Like Pion Electromagnetic Form-Factor. *Nucl.Phys.*, B277:168, 1986.
- [2] J.S. Conway, C.E. Adolphsen, J.P. Alexander, K.J. Anderson, J.G. Heinrich, et al. Experimental Study of Muon Pairs Produced by 252-GeV Pions on Tungsten. *Phys.Rev.*, D39:92–122, 1989.
- [3] P. Bordalo et al. Observation of a Nuclear Dependence of the Transverse Momentum Distribution of Massive Muon Pairs Produced in Hadronic Collisions. *Phys.Lett.*, B193:373, 1987.
- [4] B. Betev et al. Differential Cross-section of High Mass Muon Pairs Produced by a 194-GeV/ π^- Beam on a Tungsten Target. *Z.Phys.*, C28:9, 1985.
- [5] P. C. Barry, N. Sato, W. Melnitchouk, and Chueng-Ryong Ji. First Monte Carlo Global QCD Analysis of Pion Parton Distributions. *Phys. Rev. Lett.*, 121(15):152001, 2018.
- [6] I. Novikov et al. Parton Distribution Functions of the Charged Pion Within The xFitter Framework. *Phys. Rev. D*, 102(1):014040, 2020.
- [7] P. C. Barry, Chueng-Ryong Ji, N. Sato, and W. Melnitchouk. Global QCD analysis of pion parton distributions with threshold resummation. *arXiv:2108.05822*, 8 2021.
- [8] M. Aicher, A. Schafer, and W. Vogelsang. Soft-gluon resummation and the valence parton distribution function of the pion. *Phys.Rev.Lett.*, 105:252003, 2010.
- [9] A.V. Efremov and A.V. Radyushkin. Factorization and Asymptotical Behavior of Pion Form-Factor in QCD. *Phys.Lett.*, B94:245–250, 1980.
- [10] G. P. Lepage and S. J. Brodsky. Exclusive Processes in Perturbative Quantum Chromodynamics. *Phys.Rev.*, D22:2157, 1980.
- [11] J. D. Sullivan. One pion exchange and deep inelastic electron - nucleon scattering. *Phys. Rev. D*, 5:1732–1737, 1972.
- [12] G. M. Huber et al. Charged pion form-factor between $Q^{*2} = 0.60\text{-GeV}^{*2}$ and 2.45-GeV^{*2} . II. Determination of, and results for, the pion form-factor. *Phys.Rev.*, C78:045203, 2008.

- [13] A. C. Aguilar et al. Pion and Kaon Structure at the Electron-Ion Collider. *Eur. Phys. J. A*, 55(10):190, 2019.
- [14] J. Arrington et al. Revealing the structure of light pseudoscalar mesons at the electron-ion collider. *J. Phys. G*, 48(7):075106, 2021.
- [15] D. P. Anderle et al. Electron-ion collider in China. *Front. Phys. (Beijing)*, 16(6):64701, 2021.
- [16] R. Abdul-Khalek et al. Science Requirements and Detector Concepts for the Electron-Ion Collider: EIC Yellow Report. *arxiv:2103.05419*, 3 2021.
- [17] M. Burkardt. Impact parameter dependent parton distributions and off forward parton distributions for $\zeta \rightarrow 0$. *Phys. Rev.*, D62:071503, 2000. [Erratum: *Phys. Rev.* D66,119903(2002)].
- [18] D. Müeller, D. Robaschik, B. Geyer, F. M. Dittes, and J. Høfejsi. Wave functions, evolution equations and evolution kernels from light ray operators of QCD. *Fortsch. Phys.*, 42:101–141, 1994.
- [19] X. Ji. Deeply virtual Compton scattering. *Phys. Rev.*, D55:7114–7125, 1997.
- [20] X. Ji. Gauge-Invariant Decomposition of Nucleon Spin. *Phys. Rev. Lett.*, 78:610–613, 1997.
- [21] A.V. Radyushkin. Asymmetric gluon distributions and hard diffractive electroproduction. *Phys. Lett.*, B385:333–342, 1996.
- [22] A.V. Radyushkin. Nonforward parton distributions. *Phys. Rev.*, D56:5524–5557, 1997.
- [23] T. Frederico, E. Pace, B. Pasquini, and G. Salme. Pion Generalized Parton Distributions with covariant and Light-front constituent quark models. *Phys. Rev.*, D80:054021, 2009.
- [24] C. Mezrag, H. Moutarde, and F. Sabatié. Test of two new parameterizations of the Generalized Parton Distribution *H*. *Phys. Rev.*, D88:014001, 2013.
- [25] C. Mezrag, H. Moutarde, J. Rodríguez-Quintero, and F. Sabatié. Towards a Pion Generalized Parton Distribution Model from Dyson-Schwinger Equations. *arXiv:1406.7425*, 2014.
- [26] C. Mezrag, L. Chang, H. Moutarde, C.D. Roberts, J. Rodríguez-Quintero, et al. Sketching the pion’s valence-quark generalised parton distribution. *Phys. Lett.*, B741:190–196, 2014.
- [27] C. Mezrag, H. Moutarde, and J. Rodríguez-Quintero. From Bethe-Salpeter Wave functions to Generalised Parton Distributions. *Few Body Syst.*, 57(9):729–772, 2016.
- [28] C. Fanelli, E. Pace, G. Romanelli, G. Salme, and M. Salmistraro. Pion Generalized Parton Distributions within a fully covariant constituent quark model. *Eur. Phys. J. C*, 76(5):253, 2016.
- [29] M. Rinaldi. GPDs at non-zero skewness in ADS/QCD model. *Phys. Lett. B*, 771:563–567, 2017.
- [30] N. Chouika, C. Mezrag, H. Moutarde, and J. Rodríguez-Quintero. Covariant Extension of the GPD overlap representation at low Fock states. *Eur. Phys. J.*, C77:906, 2017.
- [31] N. Chouika, C. Mezrag, H. Moutarde, and J. Rodríguez-Quintero. A Nakanishi-based model illustrating the covariant extension of the pion GPD overlap representation and its ambiguities. *Phys. Lett.*, B780:287–293, 2018.
- [32] G. F. de Teramond, T. Liu, Raza Sabbir Sufian, Hans Günter Dosch, Stanley J. Brodsky, and Alexandre Deur. Universality of Generalized Parton Distributions in Light-Front Holographic QCD. *Phys. Rev. Lett.*, 120(18):182001, 2018.
- [33] C. Shi, K. Bednar, I. C. Cloët, and A. Freese. Spatial and Momentum Imaging of the Pion and Kaon. *Phys. Rev. D*, 101(7):074014, 2020.
- [34] J.-L. Zhang, Z.-F. Cui, J. Ping, and C. D. Roberts. Contact interaction analysis of pion GTMDs. *Eur. Phys. J. C*, 81(1):6, 2021.
- [35] J.-L. Zhang, K. Raya, L. Chang, Z.-F. Cui, J. M. Morgado, C. D. Roberts, and J. Rodríguez-Quintero. Measures of pion and kaon structure from generalised parton distributions. *Phys. Lett. B*, 815:136158, 2021.
- [36] S. Kumano, Q.-T. Song, and O. Teryaev. Hadron tomography by generalized distribution amplitudes in pion-pair production process $\gamma^* \gamma \rightarrow \pi^0 \pi^0$ and gravitational form factors for pion. *Phys. Rev.*, D97(1):014020, 2018.
- [37] V. Bertone, H. Dutrieux, C. Mezrag, H. Moutarde, and P. Sznajder. Deconvolution problem of deeply virtual Compton scattering. *Phys. Rev. D*, 103(11):114019, 2021.
- [38] V. Bertone, H. Dutrieux, C. Mezrag, H. Moutarde, and P. Sznajder. Shadow generalized parton distributions: a practical approach to the deconvolution problem of DVCS. In *28th International Workshop on Deep Inelastic Scattering and Related Subjects*, 7 2021.
- [39] José Manuel Morgado Chavez, Valerio Bertone, Feliciano De Soto Borrero, Maxime Defurne, Cédric Mezrag, Hervé Moutarde, José Rodríguez-Quintero, and Jorge Segovia. Pion GPDs: A path toward phenomenology. *arXiv:2110.06052*, 10 2021.
- [40] D. Binosi, L. Chang, J. Papavassiliou, S.-X. Qin, and C. D. Roberts. Symmetry preserving truncations of the gap and Bethe-Salpeter equations. *Phys. Rev. D*, 93(9):096010, 2016.
- [41] S.-X. Qin. A systematic approach to sketch Bethe-Salpeter equation. *EPJ Web Conf.*, 113:05024, 2016.
- [42] S.-X. Qin and C. D. Roberts. Resolving the Bethe-Salpeter Kernel. *Chin. Phys. Lett.*, 38(7):071201, 2021.
- [43] M. Ding, K. Raya, D. Binosi, L. Chang, C. D. Roberts, and S. M. Schmidt. Symmetry, symmetry breaking, and pion parton distributions. *Phys. Rev. D*, 101(5):054014, 2020.
- [44] M. Ding, K. Raya, D. Binosi, L. Chang, C. D. Roberts, and S. M. Schmidt. Drawing insights from pion parton distributions. *Chin. Phys. C*, 44(3):031002, 2020.
- [45] Z.-F. Cui, M. Ding, F. Gao, K. Raya, D. Binosi, L. Chang, C. D. Roberts, J. Rodríguez-Quintero, and S. M Schmidt. Kaon and pion parton distributions. *Eur. Phys. J. C*, 80(11):1064, 2020.
- [46] Z.-F. Cui, M. Ding, F. Gao, K. Raya, D. Binosi, L. Chang, C. D. Roberts, J. Rodríguez-Quintero, and S. M. Schmidt. Higgs modulation of emergent mass as revealed in kaon and pion parton distributions. *Eur. Phys. J. A*, 57(1):5, 2021.
- [47] Z. Fan and H.-W. Lin. Gluon Parton Distribution of the Pion from Lattice QCD. *arXiv:2104.06372*, 4 2021.
- [48] L. Chang and C. D. Roberts. Regarding the distribution of glue in the pion. *Chin. Phys. Lett.*, 38(8):081101, 2021.
- [49] M. Diehl. Generalized parton distributions. *Phys. Rept.*, 388:41–277, 2003.

- [50] A.V. Belitsky and A.V. Radyushkin. Unraveling hadron structure with generalized parton distributions. *Phys.Rept.*, 418:1–387, 2005.
- [51] M. Diehl, T. Feldmann, R. Jakob, and P. Kroll. The Overlap representation of skewed quark and gluon distributions. *Nucl.Phys.*, B596:33–65, 2001.
- [52] T. Frederico, G. Salme, and M. Viviani. Two-body scattering states in Minkowski space and the Nakanishi integral representation onto the null plane. *Phys. Rev.*, D85:036009, 2012.
- [53] L. Chang, I. C. Cloet, J. J. Cobos-Martinez, C. D. Roberts, S. M. Schmidt, et al. Imaging dynamical chiral symmetry breaking: pion wave function on the light front. *Phys.Rev.Lett.*, 110:132001, 2013.
- [54] J. Carbonell, T. Frederico, and V. A. Karmanov. Bound state equation for the Nakanishi weight function. *Phys. Lett.*, B769:418–423, 2017.
- [55] G. Salmé, W. de Paula, T. Frederico, and M. Viviani. Two-Fermion Bethe–Salpeter Equation in Minkowski Space: The Nakanishi Way. *Few Body Syst.*, 58(3):118, 2017.
- [56] C. Mezrag and G. Salmé. Fermion and Photon gap-equations in Minkowski space within the Nakanishi Integral Representation method. *Eur. Phys. J. C*, 81(1):34, 2021.
- [57] S.-X. Qin, C. Chen, C. Mezrag, and C. D. Roberts. Off-shell persistence of composite pions and kaons. *Phys. Rev.*, C97(1):015203, 2018.
- [58] R. J. Perry, A. Kızılersü, and A. W. Thomas. Model dependence of the pion form factor extracted from pion electroproduction. *Phys. Rev. C*, 100(2):025206, 2019.
- [59] X. Ji and J. Osborne. One loop QCD corrections to deeply virtual Compton scattering: The Parton helicity independent case. *Phys.Rev.*, D57:1337–1340, 1998.
- [60] A. V. Belitsky, D. Mueller, L. Niedermeier, and A. Schafer. Deeply virtual Compton scattering in next-to-leading order. *Phys.Lett.*, B474:163–169, 2000.
- [61] B. Pire, L. Szymanowski, and J. Wagner. NLO corrections to timelike, spacelike and double deeply virtual Compton scattering. *Phys.Rev.*, D83:034009, 2011.
- [62] H. Moutarde, B. Pire, F. Sabatie, L. Szymanowski, and J. Wagner. On timelike and spacelike deeply virtual Compton scattering at next to leading order. *Phys.Rev.*, D87:054029, 2013.
- [63] A. Bacchetta, U. D’Alesio, M. Diehl, and C. A. Miller. Single-spin asymmetries: The Trento conventions. *Phys.Rev.*, D70:117504, 2004.
- [64] B. Berthou, D. Binosi, N. Chouika, L. Colaneri, M. Guidal, C. Mezrag, H. Moutarde, J. Rodríguez-Quintero, F. Sabatié, P. Sznajder, and J. Wagner. PARTONS: PARTonic Tomography Of Nucleon Software. A computing framework for the phenomenology of Generalized Parton Distributions. *Eur. Phys. J.*, C78(6):478, 2018.
- [65] V. Bertone, S. Carrazza, and J. Rojo. APFEL: A PDF Evolution Library with QED corrections. *Comput. Phys. Commun.*, 185:1647–1668, 2014.
- [66] Valerio Bertone. APFEL++: A new PDF evolution library in C++. *PoS, DIS2017*:201, 2018.
- [67] V. Bertone and Collaborators. Revisiting evolution equations for generalised parton distributions. *In preparation*, 2021.
- [68] D. Amrath, M. Diehl, and J.-P. Lansberg. Deeply virtual Compton scattering on a virtual pion target. *Eur.Phys.J.*, C58:179–192, 2008.
- [69] A. V. Belitsky and D. Müeller. Refined analysis of photon lepton production off spinless target. *Phys.Rev.*, D79:014017, 2009.
- [70] V. M. Braun, A. N. Manashov, S. Moch, and J. Schoenleber. Two-loop coefficient function for DVCS: vector contributions. *JHEP*, 09:117, 2020.